

PAPER • OPEN ACCESS

## Distinguishing bacteria from minerals in a layered sample using time-resolved Raman spectroscopy and global analysis

To cite this article: Bram J A Mooij *et al* 2022 *J. Opt.* **24** 064007

View the [article online](#) for updates and enhancements.

You may also like

- [Orbital angular momentum underwater wireless optical communication system based on convolutional neural network](#)  
Wenqi Ma, Huimin Lu, Danyang Chen et al.
- [Development of a small power generation system with a miniature-scale swirl burner, controlled heat transfer, and thermoelectric generators](#)  
Soroush Sheykhbaglou and Seyed M Robati
- [Multi-frequency coherent perfect absorption in the one-dimensional magnetized ferrite photonic structure](#)  
Yang Zhang, Baofei Wan, Hao Zhang et al.



EDINBURGH  
INSTRUMENTS

**EXPERTS IN  
FLUORESCENCE.**

edinst.com

**FLS1000**  
PHOTOLUMINESCENCE  
SPECTROMETER



# Distinguishing bacteria from minerals in a layered sample using time-resolved Raman spectroscopy and global analysis

Bram J A Mooij<sup>1,\*</sup> , Ivo H M van Stokkum<sup>1</sup>, G R Davies<sup>2</sup> and Freek Ariese<sup>1,\*</sup>

<sup>1</sup> Department of Physics and Astronomy and LaserLaB, Faculty of Science, Vrije Universiteit Amsterdam, de Boelelaan 1085, Amsterdam, 1081 HV, The Netherlands

<sup>2</sup> Geology and Geochemistry, Faculty of Science, Vrije Universiteit Amsterdam, de Boelelaan 1085, Amsterdam, 1081 HV, The Netherlands

E-mail: [bja.mooij@gmail.com](mailto:bja.mooij@gmail.com) and [f.ariese@vu.nl](mailto:f.ariese@vu.nl)

Received 25 November 2021, revised 11 March 2022

Accepted for publication 29 March 2022

Published 4 May 2022



CrossMark

## Abstract

Mars is one of the prime candidates in the search for extraterrestrial life. At the most comparable terrestrial Martian analogue sites, life often occurs in endolithic form; i.e. hiding below the surface. To detect biomarkers of endolithic life, the two most promising options are drilling or measuring through the surface, the latter being less invasive and preferable. Raman spectroscopy is an established chemical identification method, and advanced Raman modes have been developed for sub-surface analysis. Time-resolved Raman spectroscopy (TRRS), based on picosecond pulsed excitation and a gated intensified charge-coupled device (ICCD) detector, adds the capability of fluorescence suppression and depth selection. This paper focuses on the separation of layers with time differences that are much smaller than the 200 ps full width at half-maximum gating time of the detector. As an analogue for endolithic life on Mars, *Deinococcus radiodurans* bacteria were measured through a 2.5 mm and 7.5 mm top layer of translucent calcite. TRRS spectra were recorded in a backscattering geometry, while stepwise increasing the detector delay in 25 ps steps. Through both of these layers, the Raman spectrum of the bacteria's carotenoids could be detected. Global analysis was used to model a complete time-resolved spectrum of the sample. Using this analysis, the signals could be separated into three components: mineral Raman, bacterial Raman and bacterial fluorescence. The model also corrects for gating differences across the horizontal axis of the ICCD camera. With this approach well-separated Raman spectra were obtained even for the 2.5 mm calcite layer despite the temporal separation of approximately 20 ps, which is much shorter than the 200 ps detector gating time. TRRS could be a suitable approach for non-invasive detection of extraterrestrial subsurface biomarkers.

\* Author to whom any correspondence should be addressed.



Original content from this work may be used under the terms of the [Creative Commons Attribution 4.0 licence](https://creativecommons.org/licenses/by/4.0/). Any further distribution of this work must maintain attribution to the author(s) and the title of the work, journal citation and DOI.

Supplementary material for this article is available [online](#)

Keywords: time-resolved Raman spectroscopy, extraterrestrial life, global analysis, species-associated spectra, minerals, bacteria

(Some figures may appear in colour only in the online journal)

## 1. Introduction

Mars is one of the prime candidates in the search for extraterrestrial life. Studies show that through extended periods in its history, Martian conditions were much more conducive to life than they are currently [1, 2]. Potentially, during those times life could have evolved on Mars. Another reason for looking for life on Mars is that it is physically closer to Earth than other potentially habitable planets and moons. Currently, Martian conditions are harsh and only the subsurface is considered potentially habitable [1]. Due to the thin atmosphere and lack of a magnetic field, Mars' surface is exposed to a high influx of galactic cosmic rays [3], solar energetic particles [3] and UV-C-radiation [4]. Additionally, water is sparse [5]. Therefore, only specialised extremophile life would be capable of surviving on current Mars. Mars analogue sites on Earth such as the McMurdo dry valleys in Antarctica show that in these extreme environments, life often occurs in endolithic form; life hides below the surface to protect itself from damaging radiation [6]. However, because these organisms depend on light for their energy source, the minerals above them must be translucent or transparent to transmit some of the incoming radiation. Furthermore, in the case of extinct life: biomarkers are more likely to remain intact beneath the surface.

Endolithic organisms are difficult to detect. There would be two ways of detecting signatures of life at depth: drilling through the rock and measuring the collected drill core, or measuring through the, typically translucent, mineral layer directly. Drilling on Mars is much more challenging than on Earth because of the lack of atmosphere and moisture as well as temperature fluctuations [7]. Because drilling is so challenging and in order to reduce the risk of sample contamination, the ability to measure non-invasively through a mineral layer without sample preparation would be preferable.

One of the potential methods for detecting biomarkers of life through mineral layers is Raman spectroscopy. Raman spectroscopy is a widely used technique in chemistry, Earth and life sciences. Its main advantages are a high molecular specificity and a non-destructive nature. In addition, little to no sample preparation is needed for measurements, which is especially important in its application to astrobiological research [8]. In recent years Raman instrumentation has sufficiently advanced to include a Raman spectrometer in NASA's Mars 2020 and the future launch of ESA's Exomars mission [9]. However, the conventional setups that will be included in the payload of these missions may not be the most suitable for detecting—potentially faint—life signatures through a mineral layer. The signal from superficial minerals can obscure

the signal from deeper layers and a possible fluorescence background may further reduce the detectability of the life signatures. To address these challenges, a method capable of measuring selectively through a translucent layer is required.

One of the more established methods to create higher selectivity for deeper layers is spatially-offset Raman spectroscopy (SORS) [10]. This method uses a spatial offset between the point of signal collection compared to the point of excitation. Raman photons created at greater depth are more likely to undergo multiple scattering and thus spread further laterally. The more often a single photon is scattered, the weaker the correlation between the point of excitation and its current trajectory becomes. Therefore, the ratio of Raman photons corresponding with a deeper layer relative to photons from the first layer will increase with an offset signal collection. This method has shown impressive results for instance in the field of analysing paint layers in art, distinguishing layers of only a few micrometres thickness [11]. For low-scattering samples, such as biological tissue, depths up to several millimetres can be achieved [12]. However, the approach does not suppress background fluorescence from the mineral matrix or the target material. SORS will only help to suppress fluorescence from the surface, but fluorescence photons created deeper inside the material will follow similar trajectories to the Raman photons and will therefore not be selectively suppressed.

An alternative method for obtaining depth selectivity is time-resolved Raman spectroscopy (TRRS). In a back-scattering geometry, Raman photons created deeper inside a sample will reach the detector later than Raman photons created at the surface. Therefore, a depth profile can be constructed using a time-gated detector in combination with a pulsed excitation laser. Compared to SORS, TRRS may offer a better fluorescence suppression. Matousek *et al* [13] used Kerr gating to create a time-resolved setup with a gating time of about 4 ps. This technique offers excellent temporal selectivity, but very high laser intensities are required to drive the Kerr gate and as a result the laser repetition rate is significantly limited. Note that time-resolved Raman spectra may be broadened due to the uncertainty principle: at pulse durations of 1 ps or shorter, the spectral resolution will be significantly affected. Rojalin *et al* [14] reported on a commercial TRRS setup based on a Complementary Metal Oxide Semiconductor (CMOS) single-photon avalanche diode (SPAD) detector technology for fluorescence rejection. More recently, Blacksborg *et al* developed a time-gated Raman system specifically for planetary science [15]. There have also been applications in biomedical imaging [16], mineral imaging [17] and pharmaceuticals [18]. SPAD arrays are cost-effective, but the technology

has faced numerous challenges when it comes to uniformity, efficiency, noise performance and a limited pixel count [19]. However, the technology is improving rapidly [19, 20] and approaching charge-coupled device (CCD) detectors in terms of noise performance and pixel counts [19, 21]. Recently the first  $1024 \times 1000$  SPAD detector was developed [22]. Timing uniformity, however, is still an issue [19], and in this respect the more established method of intensified charge-coupled device (ICCD) cameras is still superior to SPADs. The reason is that the intensifier is essentially a single gate for all pixels, whereas every SPAD pixel functions as a separate detector. A Raman spectrometer based on an ICCD has already been sent to Mars, in the SuperCam instrument suite on the MARS2020 mission [23]. This system can perform standoff TRRS and laser-induced breakdown spectroscopy with a gating time of 100 ns. The main aim of this time gating is to minimise the ambient light background, but it also suppresses very long-lived luminescence ( $>100$  ns) [23]. Mineral fluorescence lifetimes can range from nanoseconds to the microsecond range [24]. However, fluorescence of organic origin typically has lifetimes in the order of nanoseconds [25].

In our laboratory, a setup was developed based on an ICCD. The gating time of the ICCD is typically  $(200 \pm 10)$  ps full width at half-maximum (FWHM), depending on the position on the ICCD. By changing the electronic settings of the intensifier, the gating time can be adjusted from roughly 100 ps to continuous; but with a reduced sensitivity at shorter gating times as discussed in Efremov *et al* [26]. The current 200 ps gating time has been demonstrated to offer efficient suppression of the fluorescence background if the latter has a lifetime in the order of nanoseconds [25, 26]. Furthermore, the setup was used for a number of different depth-Raman applications: detection of explosives through non-transparent polymer container materials [27] and the discrimination between layers of minerals [28]. The setup was then used to explore whether or not life signatures from bacteria could be detected through mineral layers, with the aim for potential application in future planetary missions. In these experiments, typical carotenoid bands were observed in the TRRS spectra of *Deinococcus radiodurans* bacteria hidden behind 5 mm of translucent mineral [29]. *D. radiodurans* is well known for its strong resistance to ionising radiation and survived for an extended period of time in space [30], making it a good analogue for potential life on Mars. In the case of strongly fluorescent bacteria, the ICCD setup also showed an improvement in background suppression relative to non-gated detection [31]. However, if the time difference between layers is much smaller than the detector time gate (in the case of a thinner first layer or limited scattering), temporal separation of the signals originating from different sample layers remains a challenge. Additionally, the temporal response is not uniform over the entire detector, further increasing the difficulty of distinguishing signals from different sample layers.

To extract all information obtained from measurements with our system, data analysis is essential. We apply the global data analysis methods described in [32]. This analysis involves modelling multiple components to fully explain the sample's

spectral- and temporal response. Through an iterative optimisation algorithm, a species associated spectrum (SAS) and time response for each component are estimated. The number of distinguishable components, i.e. components with different time signatures, reveals information about the number of actual compounds contributing to the signal. Analysing the spectra of these different components helps determine whether or not bacteria were present in the sample.

To distinguish layers that are only a few millimetres apart, we need to distinguish signals that are approximately 20 ps apart, which is much shorter than the gating time of the detector. In this study, we illustrate the capabilities of the method by applying it to a challenging sample containing a calcite top layer of only 2.5 mm thickness and a bacterial second layer, mimicking endolithic life.

## 2. Materials and methods

### 2.1. Materials

Wildtype *D. radiodurans* were grown in nutrient broth (BD Bacto™ Tryptic Soy Broth,  $30 \text{ g l}^{-1}$ , Fischer-Scientific Company L.L.C., Pittsburgh, USA) at  $30^\circ\text{C}$  with agitation (200 rpm), until the stationary phase was reached. To isolate the bacteria, this suspension was centrifuged (4000 g for 10 min) and the remaining fluid was drained. Then, the bacteria were suspended in a 0.9% NaCl buffer solution, and centrifuged again at the same settings. This washing step was repeated four times to yield a pure bacterial paste. A white light image of the bacteria was recorded using a Leica DM2500 microscope with 40X objective, see supplementary figure S1 (available online at [stacks.iop.org/JOpt/24/064007/mmedia](https://stacks.iop.org/JOpt/24/064007/mmedia)).

### 2.2. Setup

The optical part of the TRRS setup is illustrated in figure 1. The laser source (Paladin Advanced 532, Coherent Inc., Santa Clara, CA, USA) has a 532 nm wavelength, 20 W average power, 76 MHz repetition rate, and 10 ps pulse duration. This wavelength was chosen in order to make use of resonance enhancement of the carotenoids in the bacteria [31]. A small portion of the light is reflected to a trigger diode via a beam sampler (BSF10-A, Thorlabs GmbH, Bergkirchen, Germany), this serves to trigger the detector. The trigger diode can be physically moved using a linear translation stage (X-LSQ-150B, Zaber Technologies Inc., Vancouver, BC, Canada) to induce very precise ( $<0.01$  ps) small delays (0–50 ps) and is connected to the detector through an electronic delay generator. The electronic delay generator contains various lengths of wire, which are electronically combined to construct a signal path with between 0 and 20000 ps length with 25 ps steps. A rotatable  $\lambda/4$ -plate in combination with a polarising beam splitter allows accurate control of the laser power. The light is reflected via a dichroic mirror towards the objective (TL2X-SAP,  $2\times$ , NA = 0.1, Thorlabs GmbH, Bergkirchen, Germany) and sample. The Raman signal is then collected using the same objective, filtered

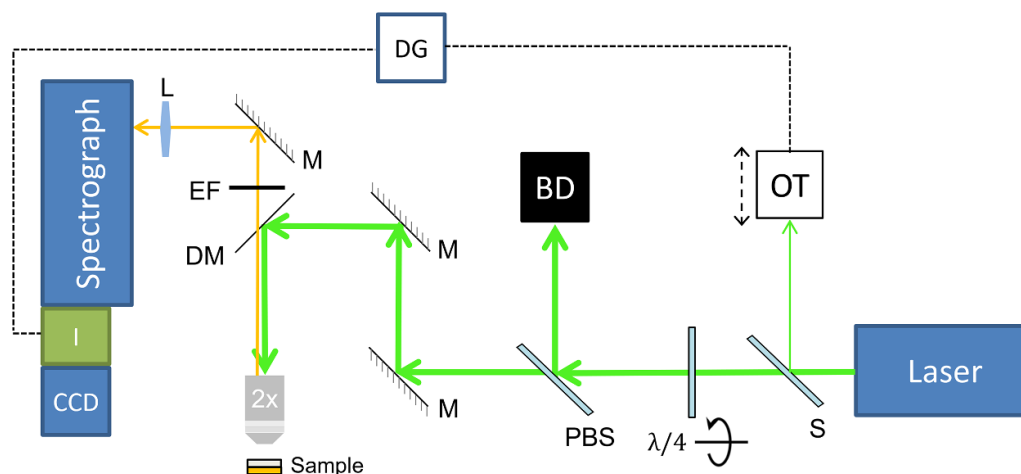


**Figure 1.** A simplified illustration of the analytical setup. Laser: 532 nm, 10 ps, 76 MHz pulsed laser. S: beam sampler ( $\sim 1\%$ ), OT: moveable optical trigger; DG: electronic delay generator  $\lambda/4$ : rotatable quarter  $\lambda$  plate; PBS: polarising beam-splitter; BD: beam dump; M: mirror; DM: dichroic mirror; 2 $\times$ : 2 $\times$  objective EF: edge filter; L: lens; I: intensifier; CCD: charge-coupled device.

by the dichroic mirror and edge filter (LPD02-532RU-25 and LP03-532RU-25, Semrock Inc., Rochester, NY, USA), focused onto the entrance slit of a spectrograph (SpectraPro 50 cm, Acton, MA, USA), and detected using a time gated CCD camera (LaVision Picostar HR, Göttingen, Germany).

The time gating relies on an intensifier in front of the CCD camera. The intensifier uses a multi-channel plate (MCP) to multiply the electrons created at the photocathode after which the electrons are converted back to photons by a phosphor screen. The intensifier can be rapidly switched on and off at 76 MHz by changing the relative voltages between the photocathode and MCP. Using an optical trigger, the detector gate timing can be defined relative to the excitation pulse. Therefore, photons only result in a CCD signal at a specified delay relative to the laser pulse. The CCD itself is continuously active, with a typical exposure time of several seconds.

### 2.3. Optical delay

While this setup was recently redesigned, it is conceptually similar to Efremov *et al* [26], with one clear exception: the optical trigger is mechanically moveable in the new system. Moving the trigger creates an optical delay, and this can be used to reduce the effect of structural deviations of the time-profile related to the electronic delay generator and intensifier. Combining three different optical delays:  $-50$  ps;  $-25$  ps and  $0$  ps, spreads these structural effects over three different delay points, significantly reducing their effect on the final results.

To illustrate this effect, a quartz cuvette of  $40 \times 10 \times 1$  mm ( $h \times w \times d$ ) was filled with cyclohexane and measured. The clear liquid and 1 mm cuvette thickness were chosen to minimise the path length difference between the Raman signals from the front and the back regions of the cuvette. Three Raman spectra were collected at different optical delays, with 10 s accumulation time per time-step and an electronic delay range of 1000 ps in steps of 25 ps.

### 2.4. Measuring bacteria through a translucent mineral

To test the setup in a situation mimicking the detection of endolithic bacteria *in situ*, three two-layered samples were constructed. The samples consisted of a 1 mm thick quartz cuvette with 1 mm thick walls, filled with pure *D. radiodurans* bacteria, and a piece of translucent natural calcite in two thicknesses: 2.5 mm or 7.5 mm. The sample was placed in the setup, with the calcite layer as the first layer and the bacteria as the second layer. The two different samples present different challenges. The 7.5 mm calcite layer blocks significantly more light than the 2.5 mm layer, limiting the Raman signal from the bacteria, so the challenge is to detect any signal from the bacteria. This spectrum can be found in the appendix in figure S5. The biggest challenge for the 2.5 mm sample is to separate the signals from the calcite and bacterial layers in time. This sample is the main focus of this article. Assuming no multiple scattering, the time difference would be  $\sim 20$  ps. The 2.5 mm sample was measured at 21 accumulations of 10 s per step and a delay range of 950 ps in steps of 25 ps. The laser power for this sample was 200 mW. This laser power did not cause any permanent photobleaching of the sample. To increase selectivity of the signal from the deeper layer, the objective was not focused on the surface of the mineral; but deeper in the sample. This method is called defocusing SORS.

The analysis of the measurement was performed using global data analysis methods as described in van Stokkum *et al* [32]. The details are explained in the Results section.

## 3. Results

### 3.1. Temporal variation of the ICCD

The intensified CCD has the characteristic that there is some—reproducible—temporal variation between different pixels. This is because the voltage is applied to the intensifier from the sides, and there is some delay as it reaches the centre. In

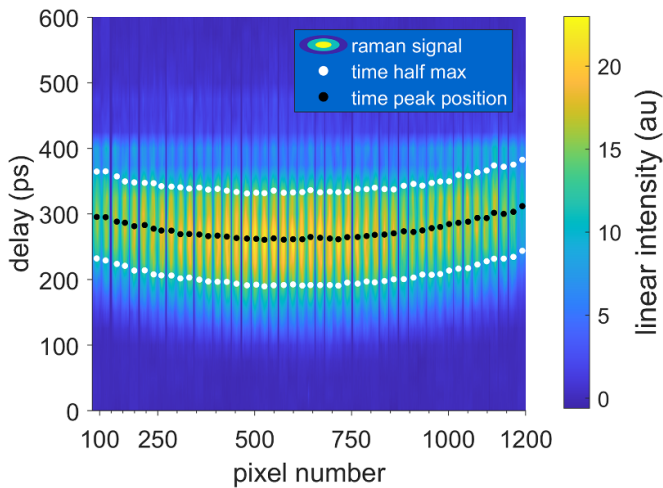


**Figure 2.** Illustration of the temporal variation of the detector response, across the horizontal axis of the ICCD in vertical binning mode. It shows the same  $1444\text{ cm}^{-1}$  Raman band of cyclohexane at various positions on the CCD, obtained by measuring a 1 mm cuvette filled with cyclohexane and measuring again after slightly rotating the grating in the spectrograph. The peaks were measured over an electronic delay range of 600 ps, with steps of 25 ps. Each  $1444\text{ cm}^{-1}$  peak in the ‘spectrum’ is represented by 23 pixels in width, selected around the highest value of the peak. The black line illustrates the mean of the time-profile for each peak. The white lines illustrate when the curve reaches half the maximum, assuming a Gaussian time-profile. Note: the pixels between the 25 ps timesteps have been linearly interpolated to give a more realistic representation of the actual time profile. There is some artefact, for instance a bright band at delay 400 ps. This is due to the delay generator and this issue is further discussed in the next section.

spectral (vertical binning) mode, this results in time differences in the order of tens of picoseconds, which cannot be neglected in our application. In a preliminary experiment, one specific cyclohexane peak was projected on various points of the ICCD detector, by a stepwise rotation of the spectrometer grating. The results are shown in figure 2. These timing differences need to be corrected for to optimise the quality and accuracy of the results.

### 3.2. Combining optical and electronic triggering

A 1 mm cuvette filled with cyclohexane was measured to illustrate the effect of combining electronic and optical delay on the instrument response function (IRF). Figure 3(a) shows three different measurements of the  $1345\text{ cm}^{-1}$  peak of cyclohexane with electronic delay on the  $x$ -axis. Each measurement was performed with a different optical delay in the path leading to the optical trigger. Measurements were performed at  $-50\text{ ps}$ ,  $-25\text{ ps}$  and  $0\text{ ps}$  optical delay. These raw curves show some structural deviations presumably related to the delay generator, see for instance the left flank at about  $225\text{ ps}$  delay. Changing the physical position of the trigger diode and combining these measurements spreads the structural noise over multiple time-points. The combined peak in figure 3(b) is more reproducible

across the spectrum and can be modelled more accurately, effectively improving the time-resolution of our measurement after data analysis.

### 3.3. Measuring bacteria through a translucent mineral

Distinguishing the multiple layers is important for selectively detecting the relatively weak spectral signatures from the potentially inhabited deeper layer among the stronger signals from the presumably lifeless top layer. We measured time-dependent Raman spectra of a 2.5 mm thick piece of calcite with a layer of *D. radiodurans* behind it. We performed 21 acquisitions of 10 s for each time step. Figure 4 shows the raw time-resolved Raman spectrum. The spectral response can be attributed to three main sources: calcite Raman peaks at  $1085\text{ cm}^{-1}$  and  $1437\text{ cm}^{-1}$ , carotenoid Raman peaks at  $1153\text{ cm}^{-1}$  and  $1512\text{ cm}^{-1}$ , and fluorescence as a broad background. The main  $1085\text{ cm}^{-1}$  calcite peak becomes visible first because this peak is an order of magnitude stronger than the others. Furthermore, the signals for calcite and carotenoids have significant overlap in time. Therefore, to accurately determine the time differences between calcite and carotenoid peaks, inspecting cross sections in time is not enough. It is necessary to combine the information of the whole spectrum to compensate for the CCD’s spatial timing differences and to minimise the systematic effect of any sampling errors. This can be achieved using global data analysis methods.

Measuring through the 7.5 mm layer of translucent calcite posed a different challenge, which was detecting any signal from *D. radiodurans*. Figure S5 shows a Raman spectrum at the delay setting with maximum Raman intensity for the carotenoid bands of *D. radiodurans*. The peaks at  $1153\text{ cm}^{-1}$  and  $1512\text{ cm}^{-1}$  are detected. Figure S6 shows a spectrum for the 2.5 mm sample measured under similar conditions.

### 3.4. Data analysis

A global analysis method was used to process the spectra. The measured time-resolved Raman spectrum is modelled as a linear superposition of three components. The model function depends upon the intrinsically nonlinear parameters  $\theta$  and conditionally linear parameters  $\varepsilon_i(\bar{\nu})$ . The parameter estimation with the help of a nonnegative least squares algorithm and the residual analysis have been described in [32–34]. The spectrum is described by:

$$\text{TRS}(t, \bar{\nu}) = c_1(t', \theta) \varepsilon_1(\bar{\nu}) + c_2(t', \theta) \varepsilon_2(\bar{\nu}) + c_3(t', \theta) \varepsilon_3(\bar{\nu}) \quad (1)$$

where  $\varepsilon_i(\bar{\nu})$  is the SAS of component  $i$  and  $c_i(t', \theta)$  describes the time-evolution of component  $i$ , with  $t' = t + t_{\text{disp}}$ . In this equation,  $t_{\text{disp}}$  is the difference between the set timing and the actual timing of the detector, see supplementary figure S4 for the modelled result.  $c_1(t', \theta)$  is assumed to be equal to the IRF, and is described by a sum of four Gaussians (11 parameters in total, location of the maximum and width of each Gaussian, plus three relative amplitudes). The IRF is well described

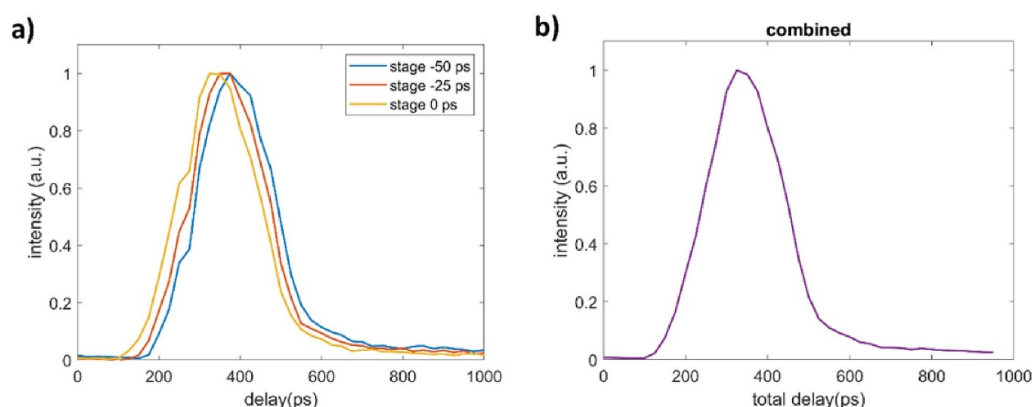


**Figure 3.** (a) A measurement of a cyclohexane peak in time (almost equal to the instrument response function), the  $x$ -axis indicates the electronic delay and the legend the optical delay. Combining the information from the three separate measurements, adding electronic and optical delay, yields figure (b). Here, the IRF is smoother and the shape is more reproducible across the spectrum and therefore it can be modelled more accurately. The shortest delay time is arbitrarily set to zero. The FWHM is approximately 200 ps.

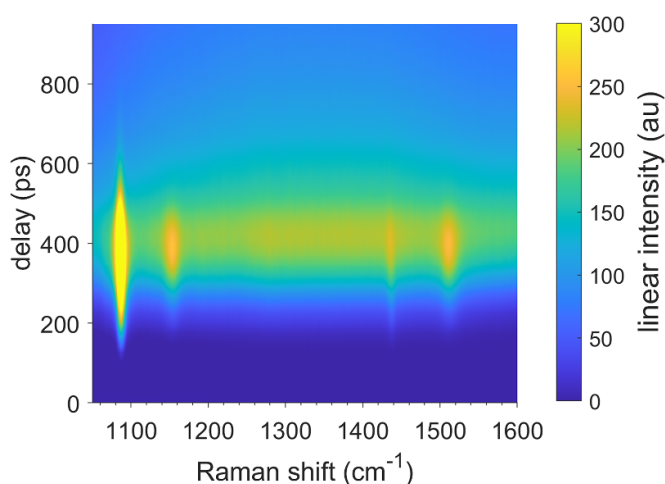


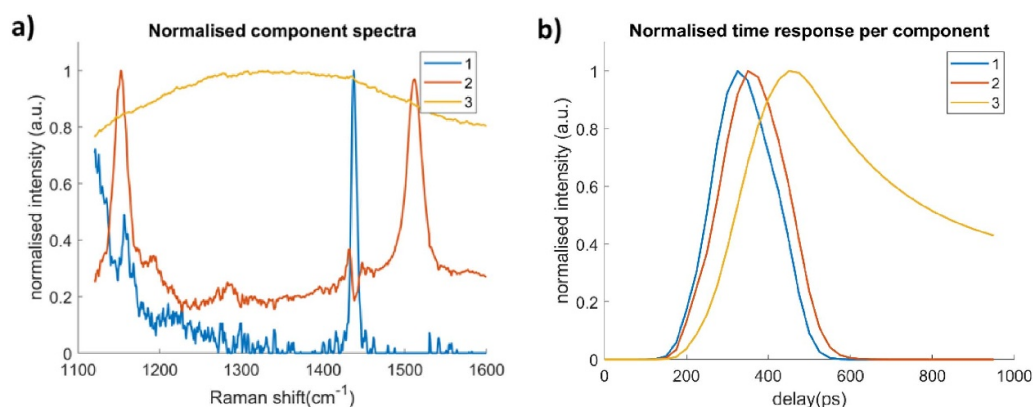
**Figure 4.** A time-resolved Raman spectrum of *D. radiodurans* behind a 2.5 mm calcite layer. The spectrum was recorded for a delay range of 950 ps with steps of 25 ps. Note: the pixels between the 25 ps timesteps have been linearly interpolated to give a more accurate representation of the actual time profile. The shortest delay time is arbitrarily set to zero. Note that the colour scale was optimised for the weaker peaks and therefore the 1085  $\text{cm}^{-1}$  calcite peak appears saturated.

by this empirical function, as evidenced by the excellent fits in figure S2, and is depicted as the blue curve in figure 5(b).  $c_2(t', \theta)$ , the red curve in figure 5(b), is described by the convolution of the IRF with an exponential decay (lifetime of 21 ps) and the third component  $c_3(t', \theta)$ , the yellow curve in figure 5(b), is described by the convolution of this IRF with a sum of two exponential decays, one with a lifetime of 239 ps and one long-lived. The data was trimmed to 1100–1600  $\text{cm}^{-1}$  to focus on the peaks of interest, and to bypass edge effects of the detector. To enhance the resolution, it has been assumed that the SAS of the calcite is zero from 1500–1530  $\text{cm}^{-1}$ , thus employing a well-known calcite characteristic [29]. In the case of an unknown mineral, this assumption can still be justified as very few minerals show Raman lines in this wavenumber

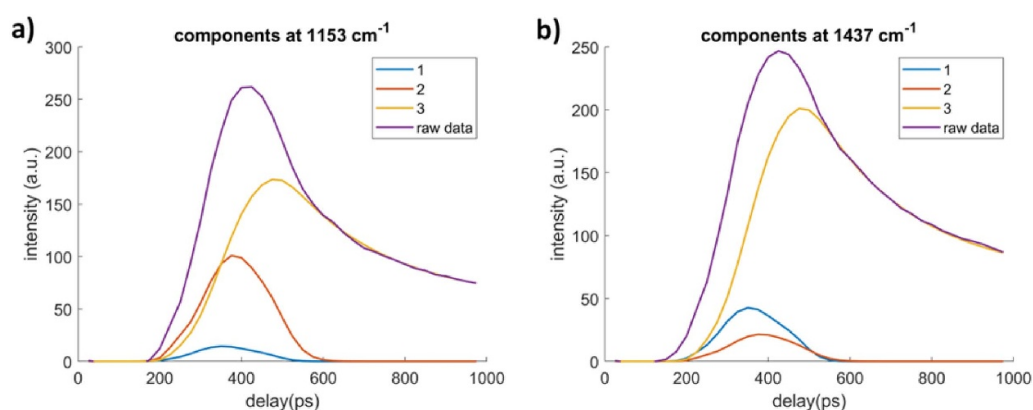
range [35]. The model describes the measured data accurately and the quality of fit is very good, see supplementary figures S2 and S3.

Figure 5 shows the estimated SAS for the three different components. Because they are independently modelled, the three species can be physically interpreted. The first component (blue) corresponds to the Raman spectrum of calcite (characterised by the peak around 1437  $\text{cm}^{-1}$ ), the second component (red) to the Raman spectrum of the carotenoids in the *D. radiodurans* bacteria (characterised by the peaks around 1153  $\text{cm}^{-1}$  and 1512  $\text{cm}^{-1}$ ) and the third component (yellow) corresponds to the fluorescence signal from the bacteria. The calcite component is modelled with a time-response equal to the IRF, while the modelled carotenoid component has a lifetime of 21 ps. We attribute this to multiple scattering, the effect of which increases with depth.

Figure 6(a) shows the relative contributions to the carotenoid peak at 1153  $\text{cm}^{-1}$  as a function of time. The sum of components 1–3 is our total model for the raw data. The relative contributions are compared at 350 ps, which is approximately the delay time of maximum intensity for the carotenoid component. Note that the fluorescence component peaks roughly 100 ps later. The major contribution (51% at 350 ps) is from component 3 (fluorescence). The second largest contribution is from component 2 (carotenoid Raman, 43% at 350 ps). Component 1 (calcite Raman) has a small contribution (6% at 350 ps) to the signal at 1153  $\text{cm}^{-1}$ . Figure 6(b) shows the relative contributions to the calcite peak at 1437  $\text{cm}^{-1}$ . Again, the major contribution (69% at 350 ps), is from component 3 (fluorescence), component 1 (calcite Raman) is the second strongest (21% at 350 ps) and there is a smaller contribution (11% at 350 ps) from component 2 (carotenoid Raman). For this specific peak there is some crosstalk between components 1 and 2, but nevertheless there is a clear separation, confirming the conclusion that component 1 corresponds to the calcite Raman signal (top layer) and component 2 to the carotenoid Raman signal of the 2nd layer.



**Figure 5.** The normalised species associated spectra of the sample of *D. radiodurans* bacteria behind 2.5 mm calcite (a) and the corresponding time signatures (b). Key: 1 blue, calcite; 2 red, bacterial carotenoids; 3 yellow, bacterial fluorescence.



**Figure 6.** Contributions of the three components to the signal at Raman shifts of 1153 cm<sup>-1</sup> (a) and 1437 cm<sup>-1</sup> (b). Key: purple, raw data; 1 blue, calcite; 2 red, bacterial carotenoids; 3 yellow, bacterial fluorescence.

#### 4. Discussion and conclusion

For detecting (traces of) life it is preferred to measure without interfering with the sample. One of the ways to achieve this is to measure directly through minerals. Spectrally separating the lifeless top layer(s) from the potentially life-containing layers beneath improves the chances of successfully detecting life signatures. The most common Raman method for depth selectivity is SORS. This method is relatively straightforward and affordable to implement and yields good separation of signals from different layers in various applications. However, when strong fluorescence is present, the Raman signal becomes obscured and may be obscured in the shot noise of the fluorescence background. TRRS allows measurements through the mineral layer, and also provides depth information. In addition, TRRS suppresses fluorescence and ambient light, which improves the detection capabilities compared to non-gated Raman methods. As many minerals exhibit strong fluorescence, fluorescence suppression is an essential part of a Raman instrument to find life on Mars. In this work, we used TRRS with excitation at 532 nm, offering (pre)-resonance enhancement for the carotenoid compounds present in *D. radiodurans*. The fluorescence background associated with visible excitation is effectively suppressed. This

makes time-resolved detection a promising Raman spectroscopy technique for finding life on Mars.

In this study, we measured *D. radiodurans* through a translucent calcite layer as an analogue for detecting life on Mars through a lifeless mineral top layer. Through 2.5 mm and 7.5 mm of translucent calcite, we were able to successfully detect a carotenoid signal from the bacteria. These mineral thicknesses were chosen to roughly correspond with the depth at which organisms might survive on Mars: not too close to the surface because of harmful radiation, not too deep in order to still collect some sun light for photosynthesis. Both photosynthesis and TRRS will depend in a similar way on the attenuation coefficient of the top mineral layer due to scattering and absorption losses. In an earlier study, a depth of 10 mm was reached through top layers of calcite and 40 mm through transparent halite [28]. Greater depths could be achieved with higher laser powers and longer measurement times. The global data analysis methods allowed us to distinguish different layers in the sample, successfully separating the mineral signal from the biomarker signal, despite these signals being much closer together than the gating time of the ICCD detector. The analysis also corrects for the non-uniform temporal response of the detector. By separating the signal from the surface and deeper layers, the method is optimised for biomarker detection

in the 2nd layer. Furthermore, time-resolved Raman measurements can be performed without interfering with the natural environment of the sample, reducing the probability of contamination and alteration of the sample. In this study, the time difference between the signal from the 1st and 2nd layer was approximately 20 ps for a 2.5 mm calcite layer. For minerals with a higher scattering coefficient this timing difference would increase and a 2nd layer would be easier to distinguish with TRRS. In this study, we detected a second layer that was laterally homogeneous, but the technology could also be used for multiple layers or for heterogeneous samples. In the past we have used a similar TRRS setup on such samples [28, 36]. In principle, if the heterogeneous material has the same SAS, but a more complicated concentration profile  $c(t)$ , one can model this  $c(t)$  with additional parameters. For example, for the bacterial fluorescence we employ a sum of two exponential decays (convolved with the IRF). As far as we are aware, global analysis has not yet been tested on such 2D-TRRS data.

With technological advances in both time-gated detectors [19, 20] and pulsed lasers [37], TRRS is becoming more accessible and more robust. Combining these developments with the methods described in this paper can push the state of the art for layer separation in TRRS. Expecting a gradual reduction in hardware weight and power consumption, we conclude that TRRS could become a valuable tool for detecting endolithic life (or subsurface biomarkers of extant life) on Mars and other extraterrestrial sites.

### Data availability statement

The data that support the findings of this study are available upon reasonable request from the authors.

### Acknowledgments

This research has been funded by the Netherlands Space Office, project ALW-GO/15-19. The laser setup was funded by the Dutch Research Council NWO, project 700.59.103. The authors acknowledge the AIMSS institute at the Vrije Universiteit Amsterdam and specifically Lucas Patty and Marijke Wagner for their help and guidance growing the bacteria.

### ORCID iD

Bram J A Mooij  <https://orcid.org/0000-0002-9705-064X>

### References

- [1] Westall F, Loizeau D, Foucher F, Bost N, Bertrand M, Vago J and Kminek G 2013 Habitability on Mars from a microbial point of view *Astrobiology* **13** 887–97
- [2] Cang X and Luo W 2019 Noachian climatic conditions on Mars inferred from valley network junction angles *Earth Planet. Sci. Lett.* **526** 115768
- [3] Hassler D M *et al* 2014 Mars' surface radiation environment measured with the Mars Science Laboratory's curiosity rover *Science* **343** 1244797
- [4] Cockell C S, Catling D C, Davis W L, Snook K, Kepner R L, Lee P and McKay C P 2000 The ultraviolet environment of Mars : biological implications past, present, and future *Icarus* **359** 343–59
- [5] Cockell C S *et al* 2016 Habitability: a review *Astrobiology* **16** 89–117
- [6] Wynn-Williams D D and Edwards H G M 2002 Environmental UV radiation: biological strategies for protection and avoidance *Astrobiology: the Quest for the Conditions of Life* (Berlin: Springer) pp 245–60
- [7] Zacny K and Cooper G 2006 Considerations, constraints and strategies for drilling on Mars *Planet. Space Sci.* **54** 345–56
- [8] Villar S E J and Edwards H G M 2006 Raman spectroscopy in astrobiology *Anal. Bioanal. Chem.* **384** 100–13
- [9] Rull F *et al* 2011 Exomars Raman laser spectrometer for Exomars *Instruments, Methods, and Missions for Astrobiology XIV* (California, United States) vol 8152 R B Hoover, P C W Davies, G V Levin and A Y Rozanov pp 138–50
- [10] Matousek P, Morris M D, Everall N, Clark I P, Towrie M, Draper E, Goodship A and Parker A W 2005 Numerical simulations of subsurface probing in diffusely scattering media using spatially offset Raman spectroscopy *Appl. Spectrosc.* **59** 1485–92
- [11] Conti C, Botteon A, Colombo C, Pinna D, Realini M and Matousek P 2020 Advances in Raman spectroscopy for the non-destructive subsurface analysis of artworks: micro-SORS *J. Cult. Heritage* **43** 319–28
- [12] Kerssens M M, Matousek P, Rogers K and Stone N 2010 Towards a safe non-invasive method for evaluating the carbonate substitution levels of hydroxyapatite (HAP) in micro-calcifications found in breast tissue *Anal. R. Soc. Chem.* **12** 3156–61
- [13] Morris M D, Matousek P, Towrie M, Parker A W, Goodship A E and Draper E R C 2005 Kerr-gated time-resolved Raman spectroscopy of equine cortical bone tissue *J. Biomed. Opt.* **10** 014014
- [14] Rojalin T, Kurki L, Laaksonen T, Viitala T, Kostamovaara J, Gordon K C, Galvis L, Wachsmann-hogiu S, Strachan C J and Yliperttula M 2016 Fluorescence-suppressed time-resolved Raman spectroscopy of pharmaceuticals using complementary metal-oxide semiconductor (CMOS) single-photon avalanche diode (SPAD) detector *Anal. Bioanal. Chem.* **408** 761–74
- [15] Blacksberg J, Alerstam E, Cochrane C J, Maruyama Y and Farmer J D 2020 Miniature high-speed, low-pulse-energy picosecond Raman spectrometer for identification of minerals and organics in planetary science *Appl. Opt.* **59** 433–44
- [16] Yerolatsitis S *et al* 2021 Sub millimetre flexible fibre probe for background and fluorescence free Raman spectroscopy *J. Biophoton.* **14** e202000488
- [17] Romppanen S, Häkkinen H, Kekkonen J, Nissinen J, Nissinen I, Kostamovaara J and Kaski S 2020 Time-gated Raman and laser-induced breakdown spectroscopy in mapping of eudialyte and catapleite *J. Raman Spectrosc.* **51** 1462–9
- [18] Lipiäinen T *et al* 2018 Time-gated Raman spectroscopy for quantitative determination of solid-state forms of fluorescent pharmaceuticals *Anal. Chem.* **90** 4832–9
- [19] Bruschini C, Homulle H, Antolovic I M, Burri S and Charbon E 2019 Single-photon avalanche diode imagers in biophotonics: review and outlook *Light Sci. Appl.* **8** 87
- [20] Bronzi D, Villa F, Tisa S, Tosi A and Zappa F 2016 SPAD figures of merit for photon-counting, photon-timing, and imaging applications: a review *IEEE Sens. J.* **16** 3–12

- [21] Chiuri A and Angelini F 2021 Fast gating for Raman spectroscopy *Sensors* **21** 2579
- [22] Morimoto K, Ardelean A, Wu M-L, Ulku A C, Antolovic I M, Bruschini C and Charbon E 2020 Megapixel time-gated SPAD image sensor for 2D and 3D imaging applications *Optica* **7** 346
- [23] Wiens R C *et al* 2021 The SuperCam Instrument Suite on the NASA Mars 2020 rover: body unit and combined system tests *Space Sci. Rev.* **217** 4
- [24] Soleimaninejad H, Matroodi F and Tavassoli S H 2013 Raman spectroscopy of Iranian region calcite using pulsed laser: an approach of fluorescence suppression by time-gating method *J. Spectrosc.* **2013** 254964
- [25] Hanke F, Mooij B J A, Ariese F and Böttger U 2019 The evaluation of time-resolved Raman spectroscopy for the suppression of background fluorescence from space-relevant samples *J. Raman Spectrosc.* **50** 14
- [26] Efremov E V, Buijs J B, Gooijer C and Ariese F 2007 Fluorescence rejection in resonance Raman spectroscopy using a picosecond-gated intensified charge-coupled device camera *Appl. Spectrosc.* **61** 571–8
- [27] Iping Petterson I E, López-López M, García-Ruiz C, Gooijer C, Buijs J B and Ariese F 2011 Noninvasive detection of concealed explosives: depth profiling through opaque plastics by time-resolved Raman spectroscopy *Anal. Chem.* **83** 8517–23
- [28] Hooijschuur J-H, Iping Petterson E I, Davies R G, Gooijer C and Ariese F 2013 Time resolved Raman spectroscopy for depth analysis of multi-layered mineral samples *J. Raman Spectrosc.* **44** 1540–7
- [29] Verkaaik M F C, Hooijschuur J, Davies G R and Ariese F 2015 Raman spectroscopic techniques for planetary exploration *Astrobiology* **15** 697–707
- [30] Kawaguchi Y *et al* 2020 DNA damage and survival time course of deinococcal cell pellets during 3 years of exposure to outer space *Front. Microbiol.* **11** 2050
- [31] Hooijschuur J H H, Verkaaik M F C F C, Davies G R R and Ariese F 2016 Will Raman meet bacteria on Mars? An overview of the optimal Raman spectroscopic techniques for carotenoid biomarkers detection on mineral backgrounds *Neth. J. Geosci.* **95** 141–51
- [32] van Stokkum I H M, Larsen D S and Grondelle R V 2004 Global and target analysis of time-resolved spectra *Biochim. Biophys. Acta* **1657** 82–104
- [33] Mullen K M and Van Stokkum I H M 2007 TIMP: an R package for modeling multi-way spectroscopic measurements *J. Stat. Softw.* **18** 3
- [34] Mullen K M and Stokkum I H M V 2009 The variable projection algorithm in time-resolved spectroscopy, microscopy and mass spectrometry applications *Numer. Algorithms* **51** 319–40
- [35] Chukanov N V and Vígassina M F 2020 *Vibrational (Infrared and Raman) Spectra of Minerals and Related Compounds* 1st edn (Berlin: Springer) (<https://doi.org/10.1007/978-3-030-26803-9>)
- [36] Iping Petterson I E, Esmonde-White F W L, de Wilde W, Morris M D and Ariese F 2015 Tissue phantoms to compare spatial and temporal offset modes of deep Raman spectroscopy *Analyst* **140** 2504–12
- [37] Shang C *et al* 2020 Review on wavelength-tunable pulsed fiber lasers based on 2D materials *Opt. Laser Technol.* **131** 106375